AGU PUBLICATIONS

Geophysical Research Letters

RESEARCH LETTER
10.1002/2015GL065837

Key Points:
- Nanoindentation of olivine was performed at 0–175°C
- Low-temperature plastic rheology of olivine was measured
- Efficacy of nanoindentation for study of mineral rheology is demonstrated

Correspondence to:
K. Kranjc,
kkranjc@wustl.edu

Citation:
Kranjc, K., Z. Rouse, K. M. Flores, and P. Skemer (2016), Low-temperature plastic rheology of olivine determined by nanoindentation, *Geophys. Res. Lett., 43*, 176–184, doi:10.1002/2015GL065837.

Received 18 AUG 2015
Accepted 14 NOV 2015
Accepted article online 24 NOV 2015
Published online 15 JAN 2016

Low-temperature plastic rheology of olivine determined by nanoindentation

Kelly Kranjc[1], Zachary Rouse[2], Katharine M. Flores[1,2], and Philip Skemer[1,3]

[1]Institute of Materials Science and Engineering, Washington University in St. Louis, St. Louis, Missouri, USA, [2]Department of Mechanical Engineering and Materials Science, Washington University in St. Louis, St. Louis, Missouri, USA, [3]Department of Earth and Planetary Sciences, Washington University in St. Louis, St. Louis, Missouri, USA

Abstract Low-temperature plasticity is a deformation mechanism that occurs mainly at high stress and low temperatures and may be important in the shallow lithosphere, at the tips of cracks, and in laboratory experiments. Previous studies investigating the low-temperature plasticity of the mineral olivine have exhibited wide variability in their extrapolations to the athermal flow strength or Peierls stress. To better constrain the rheology of olivine, nanoindentation tests were performed on samples in the temperature range of 0–175°C. The indentation properties were converted to uniaxial properties using a finite element-based method. The data were fit to a standard flow law for low-temperature plasticity, and Peierls stresses between 5.32 and 6.45 GPa were obtained. These results provide increased confidence in the extrapolation of high-pressure and high-temperature laboratory experiments to low-temperature conditions and illustrate the applicability of nanoindentation methods to the study of mineral rheology.

1. Introduction

Convection in planetary mantles is accommodated mainly by the subsolidus flow of minerals such as olivine, the most abundant mineral in the upper mantle [*Karato and Wu*, 1993]. Deformation may occur by one of several microscopic mechanisms, involving motion of dislocations, diffusive mass transfer, grain boundary sliding, or some combination thereof [e.g., *Frost and Ashby*, 1982; *Poirier*, 1985; *Karato*, 2008]. At high temperatures and low convective stresses characteristic of the sublithospheric upper mantle olivine is expected to deform by dislocation creep or by dislocation-accommodated grain boundary sliding [*Hirth and Kohlstedt*, 2003; *Hansen et al.*, 2011]. Both mechanisms produce texture, which is detected through the observation of widespread seismic anisotropy in the upper mantle [e.g., *Panning and Romanowicz*, 2006]. However, experiments show that at lower temperatures or higher stresses there is an additional contribution to deformation by power law breakdown or "low-temperature" plasticity [*Tsenn and Carter*, 1987], which may reflect a transition to obstacle-limited dislocation glide [*Kocks et al.*, 1975; *Frost and Ashby*, 1982].

It is generally assumed that the effects of low-temperature plasticity are minimal in deeper parts of the Earth when temperatures are high and convective stresses are low [*Solomatov and Moresi*, 2000; *Solomatov et al.*, 2002; *Wong and Solomatov*, 2015]. However, stresses may be larger within the ductile or semibrittle regions in the lithosphere [*Kohlstedt et al.*, 1995; *Skemer and Karato*, 2008; *Behr and Hirth*, 2014] or at the tips of cracks [*Rice and Thomson*, 1974; *Argon*, 1987]. Moreover, large shear stresses are common in laboratory experiments and the effects of low-temperature plasticity must be considered when extrapolating experimental data to geologic strain rates [*Katayama and Karato*, 2008; *Mei et al.*, 2010]. Hence, precise measurements of rheology at low temperatures are critical for interpreting geologic observations and reconciling these observations with experimental data.

In this study we present new data obtained using instrumented nanoindentation that further constrains the low-temperature rheology of olivine while demonstrating the efficacy of this technique for the general study of mineral rheology. Although indentation methods have been used extensively in fields such as materials science, [e.g., *Oliver and Pharr*, 2010], their application to geological sciences has been limited [*Barnes et al.*, 1971; *Evans and Goetze*, 1979; *Goldsby et al.*, 2004; *Broz et al.*, 2006; *Whitney et al.*, 2007; *Zhu et al.*, 2007; *Bandini et al.*, 2012]. Nanoindentation provides a number of advantages over traditional high-pressure and high-temperature rock deformation experiments. First, nanoindentation is a relatively precise technique, with subnanometer displacement resolution and force resolution as low as 100 nN [*Fischer-Cripps*, 2011, p. 263]. Second, brittle deformation is readily suppressed due to the self-confined nature of the indentation method [*Tabor*, 1970]. Hence, plasticity is easily achieved for hard materials at room temperature conditions without

secondary confinement from a gaseous or solid medium. Finally, experiments are rapid and minimally destructive, so many tests can be performed in a short period of time.

2. Background

At low-temperature conditions, obstacle-limited dislocation glide is expected to be the dominant deformation mechanism in many minerals [*Frost and Ashby*, 1982; *Tsenn and Carter*, 1987]. While there are several formulations for constitutive relations in the exponential regime, we follow here the derivation from *Frost and Ashby* [1982]. *Orowan* [1940] provided the well-known equation for strain accumulation by dislocation motion:

$$\dot{\varepsilon} = \rho b \bar{v} \tag{1}$$

which states that strain rate ($\dot{\varepsilon}$) is the product of dislocation density (ρ, itself a nonlinear function of stress), the Burgers vector of the slip system b, and the average velocity of the dislocation $\bar{v}$. A general formulation for the velocity of dislocations is

$$\bar{v} \propto \exp\left(-\frac{H^*}{RT}\right) \tag{2}$$

where H^* is the activation enthalpy, R is the gas constant, and T is the absolute temperature [*Frost and Ashby*, 1982]. In the case of low-temperature plasticity, H^* is stress dependent:

$$H^* = H_0^*\left(1 - \left(\frac{\sigma}{\sigma_c}\right)^p\right)^q \tag{3}$$

where H_0^* is the zero stress activation enthalpy, σ is the differential stress, and σ_c is the critical stress where dislocations move freely through obstacles at $T = 0$ K (the "athermal flow strength" of *Frost and Ashby* [1982]). Dimensionless constants p and q depend on the details of the energy barriers to dislocation motion and are constrained to fall within ranges $0 \le p \le 1$ and $1 \le q \le 2$ [*Kocks et al*., 1975]. For the specific case where plasticity is rate-limited by the lattice friction, $\sigma_c = \sigma_p$, where σ_p is the Peierls stress [cf. *Karato*, 2008].

Combining equations (1)–(3), and noting that ρ is proportional to σ^2, yields a constitutive expression describing low-temperature plasticity [cf. *Frost and Ashby*, 1982, equation (2.12)]:

$$\dot{\varepsilon}_{\mathrm{LTP}} = A\sigma^2 \exp\left\{-\left(\frac{H_o^*}{RT}\right)\left(1 - \left(\frac{\sigma}{\sigma_p}\right)^p\right)^q\right\} \tag{4}$$

where $\dot{\varepsilon}_{\mathrm{LTP}}$ is the strain rate of the material deforming by this mechanism and A is a material-dependent parameter. As σ/σ_p approaches unity materials begin to yield plastically at a rate that is nearly independent of temperature.

Previous studies have attempted to constrain the low-temperature behavior of olivine through microindentation [*Evans and Goetze*, 1979] and high-pressure and high-temperature deformation experiments using either Griggs or the D-DIA apparatus [*Raterron et al*., 2004; *Katayama and Karato*, 2008; *Mei et al*., 2010]. Data are fit to an equation such as equation (4), assuming particular models for dislocation obstacles. Previous studies determined Peierls stresses for dry olivine that range from 5.9 GPa [*Mei et al*., 2010] to 15.4 GPa [*Raterron et al*., 2004]; *Katayama and Karato* [2008] conducted a study under water-saturated conditions, in which they determined Peierls stresses of 1.6–2.9 GPa. Although rheological experiments at high temperature are relatively straightforward, experiments approaching room temperature are challenging due to the strength of olivine and its propensity to deform by brittle mechanisms when the applied differential stress is greater than the confining pressure [*Evans and Goetze*, 1979; *Kohlstedt et al*., 1995]. Furthermore, precise stress measurements under high confining pressures are technically difficult, requiring either in situ measurements of changes to lattice spacing with a synchrotron light source [e.g., *Raterron et al*., 2004; *Mei et al*., 2010], which have significant uncertainty [*Burnley and Zhang*, 2008], or measurements based on calibrated relationships with dislocation density [e.g., *Katayama and Karato*, 2008].

3. Experimental Procedure

3.1. Materials

Two olivine samples were investigated in this study. The first sample was derived from a single crystal of San Carlos olivine, which was separated from a mantle xenolith. Optical microscopy confirmed the sample to be free of fluid inclusions, fractures, and subgrain boundaries. A second polycrystalline sample was synthesized from ground powders of the Balsam Gap Dunite, which was vacuum sintered at 1390°C for 4 h at a pressure of 10 Pa (see *Sundberg and Cooper* [2010] for details of sample preparation). The polycrystalline olivine sample had a grain size of approximately 250 μm and no preferred crystallographic orientation. The single crystal of olivine was unoriented. Both samples are inferred to contain very low concentrations of water: San Carlos olivine is considered to be nearly anhydrous [*Li et al*., 2008], while the high-temperature preparation procedure for the polycrystalline sample should have effectively removed any preexisting water. The samples were polished to a 0.1 μm finish using diamond paste and mounted on stainless steel disks. The single crystal olivine was attached to the disk using H20E EPO-TEK silver conductive epoxy suitable for testing at elevated temperatures. The polycrystalline sample was mounted to a separate disk using cyanoacrylate adhesive, which is appropriate for room temperature testing.

3.2. Nanoindentation

Nanoindentation measurements were obtained using a Hysitron TI950 TriboIndenter outfitted with a heating/cooling stage capable of maintaining temperatures between −10 and 200°C. The sample was clamped to the heating/cooling stage, the desired temperature was set, and the sample was left to equilibrate for at least 40 min before testing. The area function, which relates indent depth to projected area, of a diamond Berkovich probe was calibrated using a fused quartz standard. The single crystal olivine sample was tested in this manner at temperatures of 0, 75, 125, and 175°C, as well as at a room temperature of 23°C without activating the temperature control stage. At least 33 indents were made at each temperature setting; a total of 175 indents were made during this part of the study. Dry nitrogen gas was flowed over the sample for the 0°C tests to prevent condensation on the sample surface. For each indent, the sample was loaded at a rate of 1000 μN/s to a maximum load of 5000 μN with a 2 s hold at maximum load.

Additional constant strain rate indentation tests were performed at room temperature at an indentation strain rate of 0.05 s^{-1}. Nanoindentation strain rate $(\dot{\varepsilon}_i)$ is calculated as the displacement rate of the nanoindentation probe divided by the instantaneous displacement [*Mayo and Nix*, 1988; *Lucas and Oliver*, 1999; *Wang et al*., 2010; *Cordova and Shen*, 2014]. During these constant strain rate tests, the load is increased exponentially over a calculated time interval to achieve the desired strain rate. A set of 16 indents performed in this manner were conducted to a maximum load of 5000 μN with a 2 s hold at maximum load and a linear unloading rate of 1000 μN/s. The nanoindentation strain rates for both the quasi-static temperature tests and the constant strain rate tests were converted to uniaxial strain rates $(\dot{\varepsilon}_u)$ through $\dot{\varepsilon}_u = \dot{\varepsilon}_i/3$, which is based on relationships found in other material systems [*Mayo and Nix*, 1988; *Poisl et al*., 1995; *Lucas and Oliver*, 1999; *Wang et al*., 2010; *Cordova and Shen*, 2014].

In order to study the effect of crystallographic orientation, tests were performed on 24 individual grains from the untextured polycrystalline olivine sample at room temperature. Approximately nine indents were performed on each of the 24 individual grains at a rate of 28 nm/s to a maximum displacement of 140 nm. All indents were placed in the center of the grains to avoid any potential influence from grain boundaries.

3.3. Data Analysis

The resulting load-displacement curves from the nanoindentation testing were first analyzed using classical relations to obtain the reduced modulus from indentation (E_r) and the hardness (H):

$$E_r = \frac{S\sqrt{\pi}}{2\sqrt{A_c}} \tag{5}$$

$$H = \frac{P_{\max}}{A_c} \tag{6}$$

where S is the slope of the load-displacement curve upon unloading, A_c is the projected contact area of the indentation, and P_{max} is the maximum indentation load. The reduced modulus was also converted into a compressive Young's modulus for an isotropic material via

$$\frac{1}{E_r} = \frac{1-\nu^2}{E} + \frac{1-\nu_i^2}{E_i} \tag{7}$$

where ν and E are the Poisson's ratio and modulus of the sample and ν_i and E_i are those of the indenter probe ($\nu_i = 0.07$, $E_i = 1140$ GPa for the diamond indenter used here). The Poisson's ratio of olivine was taken to be 0.247 for all temperatures [*Christensen*, 1996].

Each curve was further analyzed according to the method of Mata and Alcala [*Mata et al*., 2002; *Mata and Alcalá*, 2003] in order to extract uniaxial mechanical properties. This method is based on finite element modeling for nonlinear plastic deformation following the power law stress-strain relation:

$$\varepsilon = \left(\frac{\sigma_y}{E}\right)\left(\frac{\sigma}{\sigma_y}\right)^{1/n} \tag{8}$$

where σ_y is the yield strength at which plastic deformation commences, E is the Young's modulus, and n is the power law strain-hardening exponent. The von Mises yield criterion was used for their simulations. To apply Mata and Alcala's method, first a quadratic function is fit through the loading portion of the load-displacement curve in order to determine the curvature (K). The curvature is used to calculate the pile-up factor (α), a dimensionless quantity describing the amount of material pile-up or sink-in around the boundary of the probe during indentation according to the relationship

$$\alpha = \frac{K}{fH} \tag{9}$$

where f is a geometric factor equal to 24.56 for a Berkovich probe. Pileup and sink-in increase or decrease the contact area, respectively, from what is expected from the indent depth. A value of $\alpha^{0.5} > 1$ indicates the development of pile-up, while $\alpha^{0.5} < 1$ implies sink-in. E and H (from equations (6) and (7)) are then used to determine σ_r, the uniaxial stress at a total characteristic strain of 0.1, from numerical fits to finite element data [*Mata and Alcalá*, 2003, equation (5)]. Further numerical fits relate the values of σ_r, E, and $\alpha^{0.5}$ to the power law strain-hardening coefficient n [*Mata and Alcalá*, 2003, equation (7)]. Finally, E, σ_r, and n are used to calculate the yield strength of the indented material by rearranging equation (8) and applying the condition that $\varepsilon = 0.1$ when $\sigma = \sigma_r$:

$$\sigma_y = \left[\sigma_r (0.1E)^{-n}\right]^{1/1-n} \tag{10}$$

Complete details of this method are described in *Mata et al*. [2002] and *Mata and Alcalá* [2003].

Once the yield strength was obtained, the data were analyzed according to the flow law in equation (4). Several combinations of p and q were chosen to correspond with those values used in other low-temperature plasticity studies [*Evans and Goetze*, 1979; *Raterron et al*., 2004; *Katayama and Karato*, 2008; *Mei et al*., 2010]. Due to the limited data set in this study, not all of the parameters in the flow law could be constrained through a nonlinear least squares inversion. Therefore, a zero stress activation enthalpy of 320 kJ/mol, as determined by *Mei et al*. [2010], was used for the fitting process. The choice of activation enthalpy has only a minor effect on the calculated Peierls stress. This was also demonstrated by *Katayama and Karato* [2008] who found less than 10% difference in the calculated Peierls stress between activation enthalpies of 518 and 300 kJ/mol.

4. Results

The experimental conditions and results from all of the temperature tests, the constant strain rate tests, and the average values from the polycrystalline olivine are given in Table 1 with standard error from repeated measurements reported. For all of the testing conditions, the calculated $\alpha^{0.5}$ was approximately 0.88, indicating a slight sinking-in of material around the indent perimeter. This can be seen in the scanning probe microscopy (SPM) image of an example indent in Figure 1. The average strain-hardening exponent n was calculated

Table 1. Summary of Experimental Conditions and Results[a]

	Temperature (°C)	Reduced Modulus (GPa)	Hardness (GPa)	Indentation Strain Rate, $\dot{\varepsilon}_i$ ($\times 10^{-1}$ s^{-1})	Uniaxial Strain Rate, $\dot{\varepsilon}_u$ ($\times 10^{-2}$ s^{-1})	Yield Strength (GPa)
Single crystal	0	164.10 ± 7.40	14.12 ± 0.58	1.21	4.04	4.60 ± 0.27
Single crystal	23	181.29 ± 6.47	14.32 ± 0.42	1.11	3.70	4.59 ± 0.24
Single crystal[b]	23	184.27 ± 12.25	14.29 ± 0.74	0.538	1.79	4.51 ± 0.35
Single crystal	75	178.55 ± 5.22	14.91 ± 0.45	1.21	4.04	4.38 ± 0.22
Single crystal	125	160.64 ± 9.37	13.12 ± 0.55	1.20	4.01	4.28 ± 0.28
Single crystal	175	160.77 ± 9.01	13.12 ± 0.48	1.20	3.99	4.19 ± 0.32
Polycrystal	23	168.60 ± 11.53	14.42 ± 0.76	2.21	7.37	5.65 ± 0.39

[a]Standard error from repeated measurements is reported.
[b]Constant strain rate.

to be 0.22 on average for the single crystal olivine and 0.09 for the polycrystalline sample. The ratio E/σ_r, which describes the elastic and plastic contributions to the stress field under the indenter, was approximately 30 for all conditions. Figure 1, as well as all other SPM images acquired during testing, shows no evidence for crack formation at the sample surface. This indicates that all permanent deformation was accommodated by nonbrittle phenomena. Figure 2 shows the load-displacement curves for the temperature tests as well as the indentation strain rate evolution over time for a quasi-static temperature test and a constant strain rate test. The strain rate was calculated from the final 20 nm of loading for each test. A uniaxial strain rate of approximately 0.04 s^{-1} was measured for each of the temperature tests. Because this strain rate cannot be considered steady state due to the nature of the quasi-static test, constant strain rate tests were performed to ensure that the properties obtained from the quasi-static tests are valid. The constant strain rate tests exhibit less variation in measured strain rate and are in good agreement with the quasi-static tests for all of the calculated properties.

Figure 3 shows the data obtained in this study fitted to flow laws of the form given in equation (4) with (p, q) combinations of (1/2, 1), (1, 2), (2/3, 2), (3/4, 4/3), and (1, 1). The first four combinations were chosen for their use by *Mei et al.* [2010], *Raterron et al.* [2004], *Evans and Goetze* [1979], and *Frost and Ashby* [1982], respectively. The (1, 1) combination was also evaluated because it defined a lower bound for the Peierls stress [cf. *Katayama and Karato*, 2008]. Also plotted in Figure 3 are the flow laws of *Evans and Goetze* [1979], *Raterron et al.* [2004], and *Mei et al.* [2010] adjusted to a strain rate of 0.04 s^{-1}. The fitting procedure produced ~1 GPa spread in the Peierls stress, ranging from 5.32 GPa ($p = 1$, $q = 1$) to 6.45 GPa ($p = 2/3$, $q = 2$). The average room temperature yield strength measured from the polycrystalline olivine was 5.65 GPa with a standard deviation of 0.39 GPa from the orientation effects.

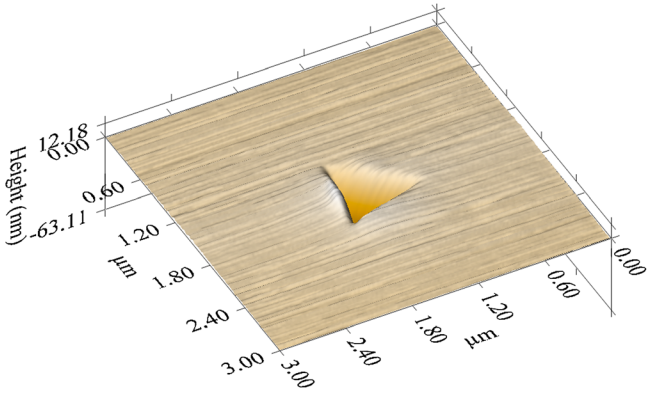

Figure 1. Scanning probe microscopy image of an indent made at 75°C. The topographical image is obtained by rastering the nanoindentation probe across the surface while maintaining a constant load between the probe and the surface. The z axis describes surface distortions relative to the height of the original surface, which is set to 0 nm. The lack of any visible cracking on the surface indicates that all permanent deformation was accommodated plastically.

5. Discussion

Figure 3 shows that the Peierls stresses determined by this study, 5.32–6.45 GPa, are among the lowest for any comparable study on dry olivine. These values are well below those determined by *Evans and Goetze* [1979] and *Raterron et al.* [2004]; however, they are in good agreement with the results of *Mei et al.* [2010], who obtained a Peierls stress of 5.9 GPa.

Because indentation tests require the activation of many independent slip systems, it is likely that the orientation of the single crystal sample had some systematic effect on the measured properties in our study. While the orientations of the samples used in this study were not determined, the

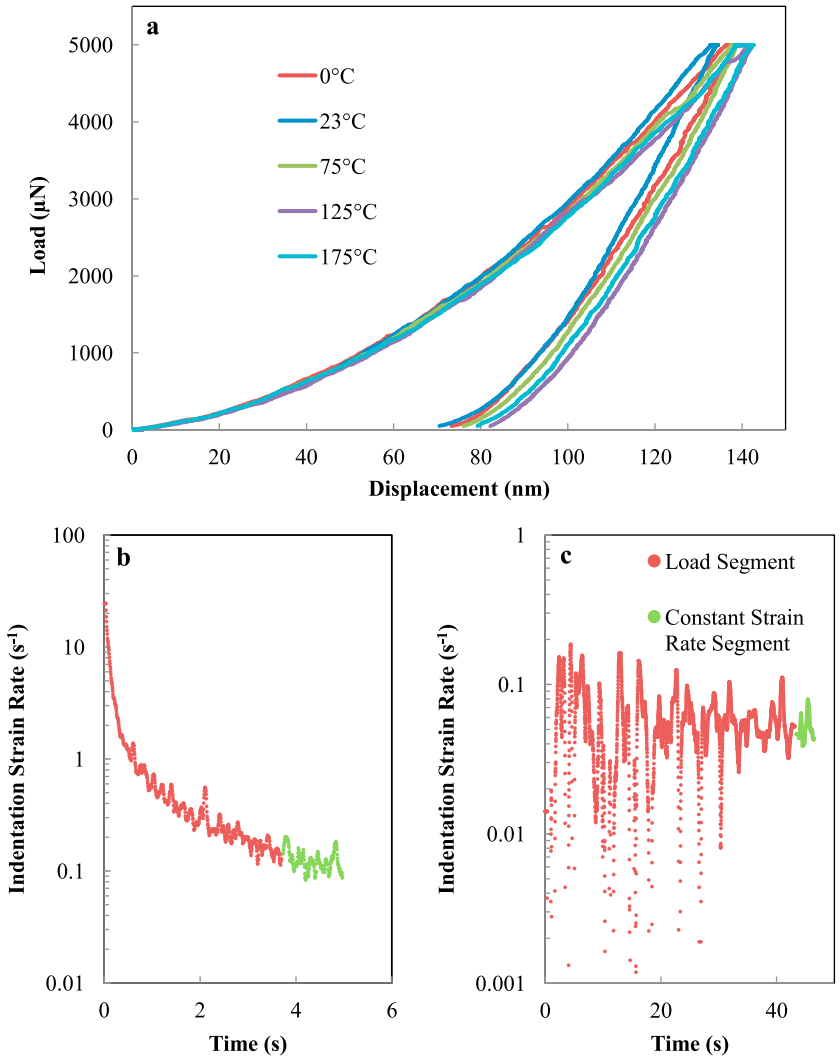

Figure 2. (a) Example of load-displacement curves from the different temperature tests. Indentation strain rate-time curves obtained at (b) 75°C for quasi-static and (c) 23°C for constant strain rate. For Figures 2b and 2c, the average strain rate over the final 20 nm of loading (constant strain rate segment; green) was used in the analysis. Each of these plots used an averaging window of 1.5% of the duration of the test. The scatter is due to fluctuations in displacement during the load-controlled testing.

indentation arrays performed in the untextured polycrystalline olivine showed that the variation in yield strength between the grains was only ~7%. Similarly, *Evans and Goetze* [1979] reported less than 10% variation in properties measured by indentation due to orientation effects. Because the testing volume of nanoindentation is well below the size of the individual olivine grains, this technique can only provide measurements of the individual grains (as if they were individual single crystals) not of the aggregate polycrystalline sample. Thus, performing the nanoindentation on a polycrystalline sample does not provide comprehensive properties for the sample as a whole. Conversely, the experiments by *Mei et al*. [2010] and *Raterron et al*. [2004] determined the average properties of an entire polycrystalline sample, which has the benefit of averaging any effects of crystallographic orientation. There is, however, a possibility that grain boundaries influenced the mechanical properties through the activation of additional deformation mechanisms.

In comparison to the high-temperature and high-pressure methods typically used to measure rheological properties of geologic materials, nanoindentation provides a relatively simple and precise method to quantify rheology in low-temperature deformation regimes. However, two particular aspects of nanoindentation

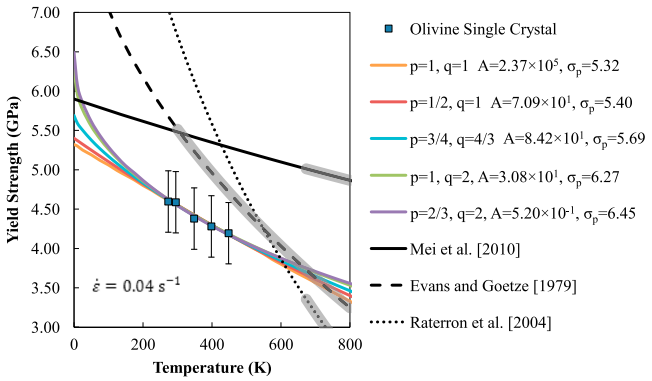

Figure 3. Yield strength plotted against temperature for the single crystal olivine tests (blue squares; $\dot{\varepsilon} = 0.04\ s^{-1}$). Each curve was plotted using $H_o^* = 320$ kJ/mol. A and σ_p given for each curve have units of $s^{-1}{\cdot}GPa^{-2}$ and GPa, respectively. The error bars on the single crystal data points reflect the potential orientation effect, which is estimated as one sigma uncertainty from the distribution of measurements on the polycrystalline sample. The single crystal olivine data were fit to Equation (4) using several combinations of p and q values. For comparison, the flow laws of *Mei et al.* [2010], *Evans and Goetze* [1979], and *Raterron et al.* [2004] at $\dot{\varepsilon} = 0.04\ s^{-1}$ are also included. The shaded gray regions on these flow laws indicate the range where experimental data were collected for each respective study.

testing that pertain to this study should be reviewed: thermal effects and conversion between indentation and uniaxial properties.

Thermal drift, the expansion or contraction between the sample and the indenter tip, is a concern at room temperature and even more so with the use of a heating or cooling stage. This drift can adversely affect the accurate measurement of the probe displacement into the sample, resulting in incorrect property measurements. While this study attempted to mitigate the effects of drift by waiting a sufficient amount of time for the sample and probe to reach thermal equilibrium, large drift rates on the order of 0.8 nm/s were observed for the 175°C testing. However, the instrument software corrects the displacement measurements to account for the measured thermal drift. Additionally, a study on thermal drift in nanoindentation reports that its effects are negligible on the computed nanoindentation modulus if the time from the beginning of the test to the start of unloading is less than $(S \cdot h_c)/\dot{P}$, where h_c is the contact depth and $\dot{P}$ is the unloading rate [*Feng and Ngan*, 2002]. At all of the temperatures tested in the current study, the test time was less than this quantity. The short test duration and automatic correction routine suggest that the effects from thermal drift on the data collected here are minimal.

The conversion of indentation measurements to uniaxial properties is not a trivial procedure. There is a very small body of literature, primarily tailored toward metals, that explores the relationship between indentation and uniaxial properties, and there is no universally applicable method to convert between the two. The uniaxial strain rate was calculated here as one third of the indentation strain rate, similar to a study by *Cordova and Shen* [2014] on Sn and a SnAgCu alloy, while other studies have found the conversion factor to be on the order of 0.1 [*Wang et al.*, 2010].

The method of calculating yield strength [*Mata and Alcalá*, 2003] also comes with some uncertainties. This method was designed for metals with any combination of yield strength in the range of 50–1000 MPa, Young's modulus in the range of 70–200 GPa, and strain-hardening exponent between 0 and 0.4. While the properties of olivine should fall within the acceptable ranges for strain-hardening exponent and Young's modulus, the yield strength falls above the intended range. The analysis depends on defining the contact under the indenter as either fully plastic or in an elasto-plastic transition. The conditions for fully plastic deformation are met when the plastic zone under the indenter is unconstrained and spreads outward from the material's free surface. This tends to be satisfied when the ratio E/σ_r is greater than 100. Applying our data to this analysis method shows that E/σ_r is around 30, meaning that the olivine indentation lies well within the elasto-plastic transition regime. The model covers E/σ_r ratios between 20 and 3000 and is applicable regardless of the deformation regime, but the calculations within the elasto-plastic regime are much more sensitive to the pile-up factor $\alpha^{0.5}$. Slight variations in this factor can greatly affect the calculated strain-hardening coefficient and, by consequence, the yield strength. However, the calculation of the pile-up factor obtained from equation (9) was verified for randomly selected indents by measuring the deformation from their SPM profiles, with less than 1% difference between the values calculated through equation (9) and measured from the SPM profile. This lends confidence to the applicability of Mata and Alcala's method to the data collected here.

6. Conclusions

Experimental determinations of mineral rheology are central to our understanding of the dynamics of Earth's interior. Here we provide data obtained using instrumented nanoindentation that constrains the rheology of olivine under conditions that favor low-temperature plasticity. These data provide increased confidence in the extrapolation of previous laboratory data to low temperatures and contribute to our basic understanding of olivine rheology at conditions relevant to the shallow lithosphere. We have demonstrated that the nanoindentation technique provides valuable data that complement traditional high-pressure and high-temperature rock mechanic experiments but also presents a number of advantages and opportunities for future research. In particular, the high precision of the stress measurements and the ability to generate large data sets mean that uncertainties in flow law parameters can be reduced significantly. Nanoindentation offers tremendous potential for micromechanical testing in parameter space previously unexplored for geologic materials.

Acknowledgments
The data obtained in this study are available for download at http://espm.wustl.edu/data. K.K. and K.F. gratefully acknowledge partial support from the Air Force Office of Scientific Research through award FA9550-12-1-0059. The authors thank Marshall Sundberg for providing the vacuum-sintered olivine sample and an anonymous reviewer for improving the clarity of the manuscript.

References

Argon, A. S. (1987), Brittle to ductile transition in cleavage fracture, *Acta Metall.*, *35*(1), 185–196, doi:10.1016/0001-6160(87)90228-8.
Bandini, A., P. Berry, E. Bemporad, and M. Sebastiani (2012), Effects of intra-crystalline microcracks on the mechanical behavior of a marble under indentation, *Int. J. Rock Mech. Min. Sci.*, *54*, 47–55, doi:10.1016/j.ijrmms.2012.05.024.
Barnes, P., D. Tabor, and J. C. F. Walker (1971), The friction and creep of polycrystalline ice, *Proc. R. Soc. London A Math. Phys. Eng. Sci.*, *324*(1557), 127–155, doi:10.1098/rspa.1971.0132.
Behr, W. M., and G. Hirth (2014), Rheological properties of the mantle lid beneath the Mojave region in Southern California, *Earth Planet. Sci. Lett.*, *393*, 60–72, doi:10.1016/j.epsl.2014.02.039.
Broz, M. E., R. F. Cook, and D. L. Whitney (2006), Microhardness, toughness, and modulus of Mohs scale minerals, *Am. Mineral.*, *91*(1), 135–142, doi:10.2138/am.2006.1844.
Burnley, P. C., and D. Zhang (2008), Interpreting in situ X-ray diffraction data from high pressure deformation experiments using elastic–plastic self-consistent models: An example using quartz, *J. Phys. Condens. Matter*, *20*(28), 285201, doi:10.1088/0953-8984/20/28/285201.
Christensen, N. I. (1996), Poisson's ratio and crustal seismology, *J. Geophys. Res.*, *101*(B2), 3139–3156, doi:10.1029/95JB03446.
Cordova, M. E., and Y. L. Shen (2014), Indentation versus uniaxial power-law creep: A numerical assessment, *J. Mater. Sci.*, *50*(3), 1394–1400, doi:10.1007/s10853-014-8699-9.
Evans, B., and C. Goetze (1979), The temperature variation of hardness of olivine and its implication for polycrystalline yield stress, *J. Geophys. Res.*, *84*(B10), 5505–5524, doi:10.1029/JB084iB10p05505.
Feng, G., and A. H. W. Ngan (2002), Effects of creep and thermal drift on modulus measurement using depth-sensing indentation, *J. Mater. Res.*, *17*(3), 660–668, doi:10.1557/JMR.2002.0094.
Fischer-Cripps, A. C. (2011), *Nanoindentation*, 3rd ed., Springer Science+Business Media, LLC, New York.
Frost, H. J., and M. F. Ashby (1982), *Deformation Mechanism Maps*, Pergamon Press, New York.
Goldsby, D. L., A. Rar, G. M. Pharr, and T. E. Tullis (2004), Nanoindentation creep of quartz, with implications for rate- and state-variable friction laws relevant to earthquake mechanics, *J. Mater. Res.*, *19*(1), 357–365, doi:10.1557/jmr.2004.19.1.357.
Hansen, L. N., M. E. Zimmerman, and D. L. Kohlstedt (2011), Grain boundary sliding in San Carlos olivine: Flow law parameters and crystallographic-preferred orientation, *J. Geophys. Res.*, *116*, B08201, doi:10.1029/2011JB008220.
Hirth, G., and D. L. D. Kohlstedt (2003), Rheology of the upper mantle and the mantle wedge: A view from the experimentalists, in *Inside the Subduction Factory*, edited by J. Eiler, pp. 83–105, AGU, Washington, D. C.
Karato, S. I. (2008), *Deformation of Earth Materials*, Cambridge Univ. Press, New York.
Karato, S. I., and P. Wu (1993), Rheology of the upper mantle: A synthesis, *Science*, *260*(5109), 771–778, doi:10.1126/science.260.5109.771.
Katayama, I., and S. I. Karato (2008), Low-temperature, high-stress deformation of olivine under water-saturated conditions, *Phys. Earth Planet. Inter.*, *168*(3–4), 125–133, doi:10.1016/j.pepi.2008.05.019.
Kocks, U. F. F., A. S. S. Argon, and M. F. F. Ashby (1975), *Thermodynamics and Kinetics of Slip*, Pergamon Press, Oxford, U. K.
Kohlstedt, D. L., B. Evans, and S. J. Mackwell (1995), Strength of the lithosphere: Constraints imposed by laboratory experiments, *J. Geophys. Res.*, *100*(B9), 17,587–17,602, doi:10.1016/S0016-0032(16)90156-X.
Li, Z. X. A., C. T. A. Lee, A. H. Peslier, A. Lenardic, and S. J. Mackwell (2008), Water contents in mantle xenoliths from the Colorado Plateau and vicinity: Implications for the mantle rheology and hydration-induced thinning of continental lithosphere, *J. Geophys. Res.*, *113*, B09210, doi:10.1029/2007JB005540.
Lucas, B. N., and W. C. Oliver (1999), Indentation power-law creep of high-purity indium, *Metall. Mater. Trans. A*, *30A*, 601–610.
Mata, M., and J. Alcalá (2003), Mechanical property evaluation through sharp indentations in elastoplastic and fully plastic contact regimes, *J. Mater. Res.*, *18*(7), 1705–1709, doi:10.1557/JMR.2003.0234.
Mata, M., M. Anglada, and J. Alcalá (2002), Contact deformation regimes around sharp indentations and the concept of the characteristic strain, *J. Mater. Res.*, *17*(5), 964–976, doi:10.1557/JMR.2002.0144.
Mayo, M. J., and W. D. Nix (1988), A micro-indentation study of superplasticity in Pb, Sn, and Sn-38 wt% Pb, *Acta Metall.*, *36*(8), 2183–2192, doi:10.1016/0001-6160(88)90319-7.
Mei, S., A. M. Suzuki, D. L. Kohlstedt, N. A. Dixon, and W. B. Durham (2010), Experimental constraints on the strength of the lithospheric mantle, *J. Geophys. Res.*, *115*, B08204, doi:10.1029/2009JB006873.
Oliver, W. C., and G. M. Pharr (2010), Nanoindentation in materials research: Past, present, and future, *MRS Bull.*, *35*(11), 897–907, doi:10.1557/mrs2010.717.
Orowan, E. (1940), Problems of plastic gliding, *Proc. Phys. Soc.*, *52*(1), 8–22, doi:10.1088/0959-5309/52/1/303.
Panning, M., and B. Romanowicz (2006), A three-dimensional radially anisotropic model of shear velocity in the whole mantle, *Geophys. J. Int.*, *167*(1), 361–379, doi:10.1111/j.1365-246X.2006.03100.x.
Poirier, J. P. (1985), *Creep of Crystals*, Cambridge Univ. Press, New York.

Poisl, W. H., W. C. Oliver, and B. D. Fabes (1995), The relationship between indentation and uniaxial creep in amorphous selenium, *J. Mater. Res.*, *10*(8), 2024–2032, doi:10.1557/JMR.1995.2024.

Raterron, P., Y. Wu, D. J. Weidner, and J. Chen (2004), Low-temperature olivine rheology at high pressure, *Phys. Earth Planet. Inter.*, *145*(1–4), 149–159, doi:10.1016/j.pepi.2004.03.007.

Rice, J. R., and R. Thomson (1974), Ductile versus brittle behaviour of crystals, *Philos. Mag.*, *29*(1), 73–97, doi:10.1080/14786437408213555.

Skemer, P., and S. I. Karato (2008), Sheared lherzolite xenoliths revisited, *J. Geophys. Res.*, *113*, B07205, doi:10.1029/2007JB005286.

Solomatov, V. S., and L. N. Moresi (2000), Scaling of time-dependent stagnant lid convection: Application to small-scale convection on Earth and other terrestrial planets, *J. Geophys. Res.*, *105*(B9), 21,795–21,817.

Solomatov, V. S., R. El-Khozondar, and V. Tikare (2002), Grain size in the lower mantle: Constraints from numerical modeling of grain growth in two-phase systems, *Phys. Earth Planet. Inter.*, *129*(3–4), 265–282, doi:10.1016/S0031-9201(01)00295-3.

Sundberg, M., and R. F. Cooper (2010), A composite viscoelastic model for incorporating grain boundary sliding and transient diffusion creep; Correlating creep and attenuation responses for materials with a fine grain size, *Philos. Mag.*, *90*(20), 2817–2840, doi:10.1080/14786431003746656.

Tabor, D. (1970), The hardness of solids, *Rev. Phys. Technol.*, *1*(3), 145–179, doi:10.1088/0034-6683/1/3/I01.

Tsenn, M. C., and N. L. Carter (1987), Upper limits of power law creep of rocks, *Tectonophysics*, *136*(1–2), 1–26, doi:10.1016/0040-1951(87)90332-5.

Wang, C. L., Y. H. Lai, J. C. Huang, and T. G. Nieh (2010), Creep of nanocrystalline nickel: A direct comparison between uniaxial and nanoindentation creep, *Scr. Mater.*, *62*(4), 175–178, doi:10.1016/j.scriptamat.2009.10.021.

Whitney, D. L., M. Broz, and R. F. Cook (2007), Hardness, toughness, and modulus of some common metamorphic minerals, *Am. Mineral.*, *92*(2–3), 281–288, doi:10.2138/am.2007.2212.

Wong, T., and V. S. Solomatov (2015), Towards scaling laws for subduction initiation on terrestrial planets: Constraints from two-dimensional steady-state convection simulations, *Prog. Earth Planet. Sci.*, *2*(1), 18, doi:10.1186/s40645-015-0041-x.

Zhu, W., J. J. Hughes, N. Bicanic, and C. J. Pearce (2007), Nanoindentation mapping of mechanical properties of cement paste and natural rocks, *Mater. Charact.*, *58*(11–12), 1189–1198, doi:10.1016/j.matchar.2007.05.018.